

Small animal PET imaging of pancreatic cancer xenografts using ^{64}Cu labeled monoclonal antibody MAb159

Hui Wang^{#1}, Dan Li^{#2,3}, Shuanglong Liu³, Ren Liu⁴, Hong Yuan¹, Valery Krasnoperov⁵, Hong Shan^{2,*}, Peter S. Conti³, Parkash S. Gill⁴, Zibo Li^{1,3*}

¹*Department of Radiology and Biomedical Research Imaging Center, University of North Carolina at Chapel Hill, Chapel Hill, North Carolina;* ²*Department of Radiology, The Third*

Affiliated Hospital of Sun Yat-sen University, Guangzhou, China; Molecular Imaging Center,

³*Department of Radiology, University of Southern California, Los Angeles, California;*

⁴*Department of Pathology, University of Southern California, Los Angeles, California; and*

⁵*Vasgene Therapeutics Inc., Los Angeles, California*

[#] H. Wang and D. Li contributed equally to this work.

Running title: PET imaging of glucose-regulated protein GRP78.

Word count: 4755

Correspondence should be sent to:

Zibo Li, PhD

Department of Radiology and Biomedical Research Imaging Center

University of North Carolina-Chapel Hill

125 Mason Farm Road

Marsico Hall, Suite 1200

North Carolina, 27599, USA

E-mail: ziboli@med.unc.edu

Hong Shan, MD, PhD

Department of Radiology

The Third Affiliated Hospital of Sun Yat-sen University

Guangzhou, 510630, China

E-mail: shanhong@mail.sysu.edu.cn

ABSTRACT

The overexpression of the GRP78 receptor on cell surface has been linked with the tumor growth, metastasis, and resistance to therapy. Based on a novel anti-GRP78 monoclonal antibody (MAb159), we developed a ^{64}Cu -labeled probe for positron emission tomography (PET) imaging of tumor GRP78 expression.

Methods: MAb159 was conjugated with the ^{64}Cu -chelator DOTA through lysine's on the antibody. DOTA-hIgG was also prepared as a control, which did not bind to GRP78. The resulting PET probes were evaluated in BxPC-3 pancreatic cancer xenografts in athymic nude mice.

Results: The radiotracer was synthesized with a specific activity of 0.8MBq/ μg antibody. In BxPC3 xenografts, ^{64}Cu -DOTA-MAb159 demonstrated prominent tumor accumulation (4.3 ± 1.2 , 15.4 ± 2.6 , and $18.3 \pm 1.0\%$ ID/g at 1, 17, and 48 post injection, respectively). In contrast, ^{64}Cu -DOTA-hIgG had low BxPC3 tumor accumulation (4.8 ± 0.5 , 7.5 ± 0.7 , and 4.6 ± 0.8 ID/g at 1, 17, and 48 h post injection, respectively).

Conclusions: We have demonstrated that GRP78 could serve as a valid target for pancreatic cancer imaging. The success of this approach would be valuable to evaluate disease course and therapeutic efficacy at the earliest stages of anti-GRP78 treatment. Moreover, these newly developed probes could have important applications in other cancer types overexpressing GRP78.

Keywords: GRP78, PET, ^{64}Cu , Pancreatic Cancer

INTRODUCTION

Pancreatic cancer (PC) is the 5th leading cause of cancer related death due to the late detection of often metastasized disease and resistance to chemotherapies (1, 2). For patients who have early disease, the best prognosis is treated surgically. Thus, new imaging methods for early detection of PC, and clinically effective method for relevant therapy response monitoring become critical factor to increase the survival in PC patients.

The glucose-regulated protein GRP78, also known as BiP (immunoglobulin heavy-chain binding protein), was discovered in the late 1970s as cellular proteins induced by glucose starvation. In human cancers, elevated GRP78 level generally correlates with higher pathologic grade, recurrence, and poor patient survival in breast, liver, prostate, colon, and gastric cancers (3). Although GRP78 expression is maintained at low basal level in major adult organs such as the brain, lung, and heart, it is strongly induced in tumors (4, 5). Besides, glucose starvation resulting from poor perfusion within tumors could induce the surface relocalization of GRP78 (3, 6, 7).

Very recently, a monoclonal antibody MAb159 against GRP78 to target surface GRP78 and block its oncogenic functions has been developed (8). MAb159 was found to suppress PI3K/AKT signaling, induce apoptosis, and induce tumor regression in xenografts and spontaneous tumor models. The humanized MAb159 retains its GRP78-binding affinity and efficacy and is nontoxic to normal organs. MAb159 is going to be tested in human in the near future.

In order to develop novel PET probe to meet the demand for the future clinical application of anti-GRP78 cancer therapy, it is desirable to develop a noninvasive PET imaging probe to

visualize and quantify GRP78 expression in vivo. Herein, we report a novel PET probe based on MAb159 and its small animal imaging results.

MATERIALS AND METHODS

Unless noted otherwise, all chemicals were of analytic grade and purchased from Sigma-Aldrich (St. Louis, MO). 1,4,7,10-Tetraazacyclododecane-1,4,7,10-tetraacetic acid (DOTA) analogs were purchased from Macrocyclics, Inc. (Dallas, TX). Size-exclusion PD-10 columns were purchased from GE Healthcare (Pittsburgh, PA). Monoclonal antibody, MAb159 was kindly provided by Vasgene Therapeutics, Inc. (Los Angeles, CA). Human IgG (hIgG) was purchased from Rockland Immunochemicals Inc. (Boyertown, PA). CD31 antibody was from BD Pharmingen (San Jose, CA). The secondary antibodies goat anti-human Alexa Fluor 568 and goat anti-rat Alexa Fluor 488 were purchased from Invitrogen (Grand Island, NY). Cy5.5 N-hydroxysuccinimide (Cy5.5-NHS) ester was purchased from Lumiprobe Corporation (Hallandale Beach, Florida, USA). ^{64}Cu was obtained from Washington University and the University of Wisconsin. ^{64}Cu was produced using the ^{64}Ni (p, n) ^{64}Cu nuclear reaction and supplied in high specific activity as $^{64}\text{CuCl}_2$ in 0.1N HCl.

Chemistry and Radiochemistry

MAb159 and hIgG were conjugated with DOTA using a method published previously (9). DOTA was first activated to DOTA-N-hydroxysulfosuccinimidyl (DOTA-NHS) as reported (10). Without purification, DOTA-NHS was cooled to 4 °C and added to the MAb159 or hIgG in 0.1 M borate buffer (pH 8.5). The reaction mixture was incubated at 4 °C for 10 h. DOTA-MAb159 or DOTA-hIgG conjugates were purified using a PD-10 column and concentrated by a Centricon filter (Millipore, Billerica, MA). The final concentration was calculated based on ultraviolet absorbance at 280 nm using unconjugated antibody of known concentrations as a standard. Both

DOTA-MAb159 and DOTA-hIgG were labeled with ^{64}Cu using the same method. 25–50 μg of the DOTA-MAb159 or DOTA-hIgG was added to $^{64}\text{CuCl}_2$ (37–74 MBq ^{64}Cu). The reaction mixture was adjusted to pH 5.5 with 0.1N sodium acetate and incubated for 1 h at 40 °C with constant shaking. The ^{64}Cu -labeled antibody conjugates were then purified by a PD-10 column using 1×PBS as the eluent. The radioactive fraction containing ^{64}Cu -DOTA-MAb159 or ^{64}Cu -DOTA-hIgG was collected for further in vitro and in vivo experiments. 5(6)-Carboxyfluorescein (FAM) -MAb159 was synthesized as reported previously (11, 12). Carboxyfluorescein succinimidyl ester (FAM-NHS) and MAb159 were mixed in the ratio of 1:1 at pH 8.5. After incubation at room temperature for 1.5 h, FAM-MAb159 was obtained after purification with PD10 column. Synthesis of Cy5.5-MAb159 and Cy5.5-hIgG were described in Supplementary Materials.

Cell Lines and Animal Model

Human pancreatic cancer cell line (BXPC3) and human lung cancer cell line (NCI-H249) were obtained from American Type Culture Collection (ATCC, Manassas, VA) and cultured under recommended conditions. Tumor models were established in 4- to 6-wk-old female athymic nude mice obtained from Harlan. Cells were used for in vitro and in vivo experiments when they reached 80-90% confluence. The GRP78 expression levels on cell lines under high- or low-glucose conditions were evaluated using western blotting. In brief, approximately 20 μg of whole-cell lysates were run on 4-20% tris-glycine gradient gel (Bio-Rad, Hercules, CA) and transferred onto nitrocellulose membrane (BioRad, Hercules, CA). The membrane was blocked with 5% non-fat dry milk in Tris Buffered Saline (TBS) and 0.05% Tween-20 (TBST) for 40 min, and then incubated with 1 $\mu\text{g}/\text{ml}$ primary antibody at 4°C overnight. Membrane was washed three times for 10 min each and incubated with secondary HRP-labeled or IRDye labeled

secondary antibody for 40 min. After three times wash with TBST, HRP signal was detected using Femto Maximum Sensitivity chemiluminescent substrate from Thermo Scientific, and IRDye signal was detected by Odyssey (LICOR, Lincoln, NE).

To generate BXPC3 tumor model, three- to five-week-old female nu/nu mice (Harlan, Indianapolis, IN) were each subcutaneously inoculated with 2×10^6 BxPC3 cells, suspended in 100 μ L of PBS, at the front flank of the mice. The tumor sizes were monitored every other day and mice were used for in vivo studies when the tumor reached 4–6 mm in diameter (typically at 3–5 weeks after inoculation of the cancer cells). The establishment of other subcutaneous tumor xenografts was described in Supplementary Materials.

In Vitro Assays

The binding affinity of DOTA-MAb159 or DOTA-hIgG to GRP78 was evaluated through the bead-based binding assay following a literature reported procedure (11, 13). The GRP78 binding activity of unmodified MAb159 and hIgG was also evaluated as a positive and negative control, respectively. Cellular uptake analysis was performed as described (14). BXPC3 tumor cells cultured in either high glucose (HG) or glucose-free (GF) DME supplemented with 10% fetal bovine serum. Ten μ g/ml FAM-MAb159 was added to BXPC3 cells. After incubation at 37 °C for 0.5 h, the cells were fixed with 2% paraformaldehyde and stained with 4'-6-diamidino-2-phenylindole (DAPI). The cell uptake images were obtained with an Eclipse 80i fluorescence microscope (Nikon).

PET Imaging and Image Analysis

PET scans and image analysis were performed using a PET R4 rodent model scanner (Siemens Medical Solutions) or eXplore Vista PET/CT rodent scanner as previously reported (10, 15). In brief, 3.7–7.4 MBq PET probe was intravenously injected into each mouse under isoflurane

anesthesia. Static scans were acquired at 1, 17, and 48h after injection. The images were reconstructed by 2-dimensional ordered-subsets expectation maximum (OSEM). For each PET scan, regions of interest (ROIs) were drawn over the tumor, normal tissue, and major organs on decay-corrected whole-body coronal images. The radioactivity concentration in each organ was obtained from the mean values within the multiple ROIs and then converted to percentage injected dose per gram of tissue (%ID/g) (16). After all PET scans were performed, the animals were sacrificed; the blood, heart and other major organs were collected and wet-weighed. The radioactivity in the tissue was measured using a gamma-counter (Packard Instruments). The results are presented as the percentage injected dose per gram of tissue (%ID/g). Values are expressed as the means \pm SD for a group of three animals.

Immunofluorescence Staining of Tumor Tissues

For the antibody distribution assay in tumor, 30 μ g of DOTA-MAb159 or DOTA-hIgG were injected via the tail vein into each mouse bearing BXPC3 tumor. At 48 h after injection, the mice were sacrificed and the tumors dissected. Frozen sections of tumors (8 μ m) were fixed in 4% paraformaldehyde (Electron Microscopy Sciences) and blocked with 10% normal goat serum (Invitrogen). Sections were then incubated with anti-CD31 primary antibody overnight at 4 °C, followed by the corresponding secondary antibody for 1 h at room temperature. Subsequently, the slides were covered with Vectashield mounting medium (Vector Labs) with 4, 6-diamino-2-phenylindole and images were obtained with an Eclipse 80i fluorescence microscope (Nikon). Secondary antibody goat anti-human Alexa Fluor 568 and goat anti-rat Alexa Fluor 488 were used to detect antibodies (hIgG or MAb159) and CD31, respectively. Preparation of HT29 and PC3 tumor sections and CD31 staining of these sections were described in Supplementary Materials.

Statistical Analysis

Quantitative data are expressed as mean \pm SD. Means were compared using 1-way ANOVA and the Student t test. *P* values of less than 0.05 were considered statistically significant.

RESULTS

Chemistry and Radiochemistry

In the DOTA conjugation reaction, 20 equivalent DOTA-NHS was added to the MAb159 or hIgG in slightly basic condition (Figure 1). After 10 h incubation at 4°C, PD10-purification afforded DOTA-MAb159 and DOTA-hIgG in 82% and 75% yield, respectively. The average number of DOTA in each antibody was not determined. ⁶⁴Cu labeling for DOTA-MAb159 and DOTA-hIgG was achieved in pH 5.5 sodium acetate solution with decay corrected yields of 56% and 42%, respectively. The specific activity of final product was estimated to be 0.8MBq/ μ g antibody.

Western Blot

Measured by Western blotting, GRP78 expression levels were determined in a human pancreatic cancer cell line (BXPC3) and a human lung cancer cell line (NCI-H249) (Figure 2). The cells were cultured in either high glucose (HG) or glucose-free (GF) DME supplemented with 10% fetal bovine serum. The glucose-free conditions was used to mimicked nutrient deprivation in the tumor microenvironment, in which greater amount of MAb159 was recruited to cancer cell surface under stress as reported (17, 18). Both BXPC3 and NCI-H249 cultured in the high glucose medium showed GRP78 expression (Figure 2A). As expected, cells cultured in glucose free medium showed more than 100% GRP78 expression when used β -actin as an internal

standard for quantification (Figure 2B). With western blot results in hand, we chose BXPC3 cell line for the following in vivo study.

In vitro Characterization of MAb159 probes

To prove that labeling DOTA did not alter the activity of MAb159, a binding affinity experiment was performed with unlabeled MAb159 as a reference. Setting MAb159 as 100%, DOTA-MAb159 retained $85.35\% \pm 4.10\%$ binding activity ($n = 3$). As a negative control, DOTA-hIgG showed negligible binding to GRP78 ($0.055 \pm 0.001\%$, $n = 3$). These result confirmed that DOTA has a minimum effect in reducing the binding affinity of MAb159 to GRP78 receptor. In addition, the cellular uptake of FAM labeled MAb159 was also tested in BXPC3 tumor cells cultured in both HG and GF medium (Figure 3). In the HG group, relatively low cell uptake was observed (Figure 3, top). In contrast, the GF group showed much higher level of FAM-MAb159 uptake (Figure 3, bottom). Considering the different expression level of GRP78 between HG and GF groups, we concluded that the FAM-MAb159 uptake was specific to GRP78 receptors.

Small-Animal PET and Image Analysis

The tumor targeting efficacy of ^{64}Cu -DOTA-MAb159 was evaluated by static small-animal PET scans in BXPC3 tumor-bearing mice. Representative decay-corrected coronal PET images at different time points are shown in Figure 4. ^{64}Cu -DOTA-hIgG was used as a negative control for side-by-side comparison. At 1 h after injection, both ^{64}Cu -DOTA-MAb159 and ^{64}Cu -DOTA-hIgG were circulating mainly in the blood pool. The BXPC3 tumors were clearly visualized in ^{64}Cu -DOTA-MAb159 group, with good tumor-to-background contrast at late time points. The activity accumulation of ^{64}Cu -DOTA-MAb159 in BXPC3 tumors was 4.3 ± 1.2 , 15.4 ± 2.6 , and

18.3 ± 1.0%ID/g at 1, 17, and 48 h p.i., respectively. On the contrary, the activity accumulation of ^{64}Cu -DOTA-hIgG in BXP3 tumors was 4.8 ± 0.5, 7.5 ± 0.7, and 4.6 ± 0.8 %ID/g at 1, 17, and 48 h p.i., respectively. Except the 1-h time point, ^{64}Cu -DOTA-MAb159 demonstrated significantly higher tumor uptake than ^{64}Cu -DOTA-hIgG ($P < 0.05$). Other than tumor uptake, both ^{64}Cu -DOTA-MAb159 and ^{64}Cu -DOTA-hIgG showed similar distribution pattern in normal organs such as liver, kidney, and muscle. At 1-h time point, tumor to muscle contrast for ^{64}Cu -DOTA-MAb159 was 1.40 ± 0.30. With the continued accumulation of ^{64}Cu -DOTA-MAb159 in BXP3 tumor, the tumor-to-muscle ratio increased to 7.4 ± 4.6 (17 h p.i.) and 11.5 ± 7.2 (48 h p.i.).

In order to further validate the PET quantification, biodistribution by direct tissue sampling was obtained right after PET scans (Figure 6). The BXP3 tumor uptake for ^{64}Cu -DOTA-MAb159 and ^{64}Cu -DOTA-hIgG was 13.1 ± 1.7, and 5.3 ± 0.6 %ID/g, respectively. In contrast, uptake for other normal organs between ^{64}Cu -DOTA-MAb159 and ^{64}Cu -DOTA-hIgG showed similar results with no significant difference ($P > 0.05$). The biodistribution results are consistent with PET quantification.

The tumor targeting efficacy of ^{64}Cu -DOTA-MAb159 was also evaluated by static small-animal PET scans in human colorectal cancer HT29 and human prostate cancer PC-3 tumor-bearing mice. The representative PET images were shown in Supplementary Figure 1. The activity accumulation of ^{64}Cu -DOTA-MAb159 in PC3 was 2.1±0.5, 3.8±0.5, and 4.2±0.1%ID/g at 1, 24, and 48h p.i., which was significantly higher than that in muscle (0.4±0.1, 0.5±0.4, and 0.2±0.1%ID/g at 1, 24, and 48 h p.i.) (Supplementary Figure 2A). Similar results were also observed in HT29 xenografts. The activity accumulation of ^{64}Cu -DOTA-MAb159 in HT29 tumor was 2.6±0.4, 4.4±1.3, and 4.5±1.3 %ID/g at 1, 24, and 48 h p.i., respectively, which was

significantly higher than that in muscle (0.4 ± 0.1 , 0.4 ± 0.1 , and 0.2 ± 0.01 %ID/g at 1, 24, and 48 h, p.i., respectively) (Supplementary Figure 2B).

Immunofluorescence Staining of Tumor Tissue

To further confirm that MAb159 targeted the GRP78 on tumor cells surface in vivo, we stained the tumor tissue using intravenously injected MAb159 as the primary antibody and goat antihuman antibody conjugated with Alexa Fluor as the secondary antibody. Images were obtained under identical conditions and displayed at the same scale so that the relative brightness observed in the images reflected the difference in relative MAb159 and hIgG concentration level (Figure 7). For MAb159, strong red signal was observed in tumor tissue, indicating the prominent accumulation of the antibody. The negative control hIgG showed minimal distribution in BXPC3 tumor. Similar results were also observed in HT29 and PC3 tumor models (Supplementary Figure 3). Both the biodistribution and immunofluorescence staining studies confirmed that MAb159 was specifically targeting GRP78 receptor.

DISCUSSION

Accumulative works have demonstrated that GRP78 protein, a master switch in ER stress, plays a pivotal role in cancer cell proliferation, angiogenesis and chemoresistance (6,19,20). GRP78 localized mainly in the endoplasmic reticulum (ER), but GRP78 can also re-locate to the cell membrane. Cell surface GRP78 expression has been detected in many different cancers, such as breast, liver, prostate and pancreatic cancer and has been associated to development of drug resistance and cell transformation(17, 21-23). These findings, coupled with the observation that peptides targeting GRP78 homed into tumor tissues but much less in normal organs suggest that cell surface GRP78 could serve as a novel target for cancer specific imaging and drug delivery.

MAb159 specifically recognizes cell surface GRP78, and thus can be used to image the tumor for personalized medicine and determine whether the amount of surface GRP78 in the tumor predicts disease progression and response to therapy. In this study, we develop a MAb159-based noninvasive PET imaging probe to visualize and quantify GRP78 expression in tumor-bearing mice *in vivo*.

In our approach, the novel ^{64}Cu -labeled MAb159 antibody was synthesized and characterized to demonstrate that imaging GRP78 expression with PET is feasible. Attachment of ^{64}Cu to MAb159 was fulfilled by using commercially available bifunctional chelators – DOTA. Binding activity assay showed that DOTA-MAb159 preserved $85.35\% \pm 4.10\%$ GRP78 binding activity as compared with unmodified MAb159. We used glucose-free conditions to mimic nutrient deprivation in the tumor microenvironment, and performed western blot to analyze GRP78 expression level in tumor cells. Western blot results demonstrated that tumor cells cultured in glucose free medium showed significantly higher GRP78 expression than the cells cultured in high-glucose medium (Figure 2). Cell uptake study further confirmed that MAb159 could bind to glucose-starving BXPC3 tumor cells, which had higher GRP78 expression level, but not to BXPC3 tumor cells cultured in HG medium, which had less GRP78 expression (Figure 3).

The *in vivo* small animal PET imaging study was performed on BXPC3 tumor xenograft mice (Figure 4 and 5). ^{64}Cu -DOTA-MAb159 and ^{64}Cu -DOTA-hIgG showed similar distribution pattern in normal organs such as liver, kidney, and muscle. However, ^{64}Cu -DOTA-MAb159 uptake in BXPC3 tumors increased with time, with maximum tumor uptake of $18.3 \pm 1.0\%$ ID/g at 48 h p.i. Both active uptake (contributed by MAb159-GRP78 interaction) and passive uptake (contributed by the enhanced permeability and retention effect) led to ^{64}Cu -DOTA-MAb159 accumulation in BXPC3 tumors. In contrast, tumor accumulation of ^{64}Cu -DOTA-hIgG was only

caused by passive uptake, with a peak uptake value of $7.5 \pm 0.7\%$ ID/g at 24 hr p.i. *Ex vivo* biodistribution further validate the PET imaging results. The BXPC3 tumor uptake for ^{64}Cu -DOTA-MAb159 and ^{64}Cu -DOTA-hIgG was 14.9 ± 0.7 , and 3.3 ± 0.6 %ID/g, respectively. Although non-targeting ^{64}Cu -DOTA-hIgG also showed some accumulation in BXPC3 tumors, the significant difference in tumor uptake between ^{64}Cu -DOTA-MAb159 and ^{64}Cu -DOTA-hIgG should be caused by the GRP78 targeting. In addition, ^{64}Cu -DOTA-MAb159 showed significantly higher tumor uptake in both HT29 and PC3 xenografts (Supplementary Figure 1) as compared with non-targeted tissue, such as muscle, which further indicated the specific GRP78 targeting of ^{64}Cu -DOTA-MAb159. In this study, we used subcutaneous tumor models. Although subcutaneous tumor models are not orthotopic and do not represent appropriate sites for human tumors, it's easy to establish; the tumor growth is predictable and reproducible. In addition, hypoxia and poor blood perfusion have been proved and measured in subcutaneous tumors by combining ultrasound and photoacoustic imaging by several independent groups (24-26). Therefore, subcutaneous xenografts models should be useful in preliminary evaluation of PET imaging of stress-induced GRP78 upregulation using ^{64}Cu -DOTA-MAb159. Although we observed prominent and specific tumor uptake with ^{64}Cu -DOTA-MAb159, we do like to point out that the DOTA chelating agents have the potential of losing ^{64}Cu from the conjugate in vivo, leading to high uptake in the liver. Other stable chelators including sarcophagine cage, NOTA, or cross-bridged chelators would be considered in our follow-up study if the agent is mainly used as a diagnosis probe. Nonetheless, DOTA has the capability to chelate other therapeutic radiometals (such as ^{177}Lu , and ^{90}Y), which may allow us translate the DOTA based imaging agent to radiotherapeutic agent by changing the radiometal to therapeutic isotopes. We used universal chelators DOTA which can complex a wide variety of both imaging and therapeutic

radioisotopes. The same DOTA-MAb159 conjugate can therefore be readily used for both imaging and therapeutic applications, without significantly altering its pharmacokinetic and tumor targeting efficacy.

It's been reported that ER stress is activated and expression of GRP78 get upregulated in both acute (27) and chronic rodent pancreatitis modes (28). Therefore, using MAb159 based molecular imaging probes may not be advantageous in differential diagnosis of pancreatic cancer and pancreatitis. However, this issue might be less significant in the clinical application of MAb159 based GRP78 imaging because GRP78 upregulation is more associated with the cancer progression and development of chemoresistance instead of early differential diagnosis of pancreatic cancer (29). After an initial response, tumors eventually became resistant to chemotherapy which accounts for the death of most cancer patients. As main regulator of cell stress, GRP78 can serve as biomarker in progressive and chemoresistant tumors. In this study, we only evaluated the feasibility of using MAb159 based PET probe for GRP78 imaging. One potential application of MAb159 based GRP78 imaging probes will be monitoring the tumor aggressiveness and chemoresistance during the treatment. Our preliminary data showed that after treatment with 50 μ M gemcitabine for 24 hours, HT29 cells demonstrated increased MAb-Cy5.5 binding (Supplementary Figure 4) and significantly increased cell uptake of ^{64}Cu -DOTA-MAb159 (Supplementary Figure 5). In contrast, the HT29 cell binding and uptake of IgG-Cy5.5 and ^{64}Cu -DOTA-IgG were unchanged or slightly decreased by gemcitabine treatment. Since the cells were not permeabilized in the experiments, the increased binding of MAb-Cy5.5 indicated that the cell surface GRP78 level increased after treatment. Although the in vitro data showed promising results, being a master switch in ER stress, GRP78 expression level will be regulated

by many factors including blood flow, tumor size, hypoxia etc. In our follow up study, more comprehensive experimental design, larger sample size, a variety of tumor models, more treatment regime, the optimal imaging windows, as well as the correlation between imaging changes and cell surface GRP78 expression will be investigated carefully in order to confirm the correlation between cell surface GRP78 and treatment results in vivo.

CONCLUSION

We have developed a receptor-targeted PET probe for detection of GRP78 upregulation in pancreatic tumor xenograft and other tumor models. This study shows that ^{64}Cu -DOTA-MAb159, based on a humanized GRP78 specific monoclonal antibody, displays high target specificity both in vitro and in vivo. The potential correlation between cell surface GRP78 expression levels and tumor chemoresistance in multiple cancer types makes ^{64}Cu -DOTA-MAb159 clinical translatable agent for monitoring the tumor progression and development of chemoresistance.

ACKNOWLEDGEMENT

This work was supported by the 1R01EB014354-01A1 (NIBIB), P30-CA016086-35-37 (NCI), the American Cancer Society (12199ss1-MRSG-12-034-01-CCE), Vasgene Therapeutics Inc. (NIH: CA168158-01; CA171538-01), National Natural Science Foundation of China (No. U1032002, 81071206, 81271621, 81301266), and Key Clinical Research Project of Public Health Ministry of China 2010-2012 (No. 164).

References:

1. Hidalgo M. Pancreatic cancer. *N Engl J Med*. 2010; 362:1605-1617.
2. Siegel R, Ma J, Zou Z, et al. *CA Cancer J Clin*. 2014; 64: 9-29.
3. Fu Y, Lee AS. Glucose regulated proteins in cancer progression, drug resistance and immunotherapy. *Cancer Biol Ther*. 2006;5:741-744.
4. Dong D, Dubeau L, Bading J, et al. Spontaneous and controllable activation of suicide gene expression driven by the stress-inducible grp78 promoter resulting in eradication of sizable human tumors. *Hum Gene Ther*. 2004;15:553-561.
5. Li J, Lee B, Lee AS. Endoplasmic reticulum stress-induced apoptosis: multiple pathways and activation of p53-up-regulated modulator of apoptosis (PUMA) and NOXA by p53. *J Biol Chem*. 2006;281:7260-7270.
6. Lee AS. GRP78 induction in cancer: therapeutic and prognostic implications. *Cancer Res*. 2007;67:3496-3499.
7. Park HR, Tomida A, Sato S, et al. Effect on tumor cells of blocking survival response to glucose deprivation. *J Natl Cancer Inst*. 2004;96:1300-1310.
8. Liu R, Li X, Gao W, et al. Monoclonal antibody against cell surface GRP78 as a novel agent in suppressing PI3K/AKT signaling, tumor growth, and metastasis. *Clin Cancer Res*. 2013;19:6802-6811.
9. Li ZB, Cai W, Cao Q, et al. (64)Cu-labeled tetrameric and octameric RGD peptides for small-animal PET of tumor alpha(v)beta(3) integrin expression. *J Nucl Med*. 2007;48:1162-1171.
10. Liu S, Li D, Huang CW, et al. Efficient construction of PET/fluorescence probe based on sarcophagine cage: an opportunity to integrate diagnosis with treatment. *Mol Imaging Biol*. 2012;14:718-724.

11. Li D, Liu S, Liu R, et al. Axl-targeted cancer imaging with humanized antibody h173. *Mol Imaging Biol.* 2014;16:511-518.
12. Li D, Liu S, Liu R, et al. EphB4-targeted imaging with antibody h131, h131-F(ab')₂ and h131-Fab. *Mol Pharm.* 2013;10:4527-4533.
13. Li D, Liu S, Liu R, et al. Targeting the EphB4 receptor for cancer diagnosis and therapy monitoring. *Mol Pharm.* 2013;10:329-336.
14. Liu S, Li D, Guo J, et al. Design, synthesis, and validation of Axl-targeted monoclonal antibody probe for microPET imaging in human lung cancer xenograft. *Mol Pharm.* 2014;11:3974-3979.
15. Liu S, Li Z, Yap LP, et al. Efficient preparation and biological evaluation of a novel multivalency bifunctional chelator for ⁶⁴Cu radiopharmaceuticals. *Chemistry.* 2011;17:10222-10225.
16. Wu Y, Zhang X, Xiong Z, et al. microPET imaging of glioma integrin $\alpha_v\beta_3$ expression using (⁶⁴)Cu-labeled tetrameric RGD peptide. *J Nucl Med.* 2005;46:1707-1718.
17. Ni M, Zhang Y, Lee AS. Beyond the endoplasmic reticulum: atypical GRP78 in cell viability, signalling and therapeutic targeting. *Biochem J.* 2011;434:181-188.
18. Zhang Y, Liu R, Ni M, et al. Cell surface relocation of the endoplasmic reticulum chaperone and unfolded protein response regulator GRP78/BiP. *J Biol Chem.* 2010;285:15065-15075.
19. Li J, Lee AS. Stress induction of GRP78/BiP and its role in cancer. *Curr Mol Med.* 2006;6:45-54.
20. Li Z. Glucose regulated protein 78: a critical link between tumor microenvironment and cancer hallmarks. *Biochim Biophys Acta.* 2012;1826:13-22.

21. Dong D, Stapleton C, Luo B, et al. A critical role for GRP78/BiP in the tumor microenvironment for neovascularization during tumor growth and metastasis. *Cancer Res.* 2011;71:2848-2857.
22. Virrey JJ, Dong D, Stiles C, et al. Stress chaperone GRP78/BiP confers chemoresistance to tumor-associated endothelial cells. *Mol Cancer Res.* 2008;6:1268-1275.
23. Wey S, Luo B, Tseng CC, et al. Inducible knockout of GRP78/BiP in the hematopoietic system suppresses Pten-null leukemogenesis and AKT oncogenic signaling. *Blood.* 2012;119:817-825.
24. Shao Q, Morgounova E, Jiang C, et al. In vivo photoacoustic lifetime imaging of tumor hypoxia in small animals. *J Biomed Opt.* 2013;18:076019.
25. Lungu GF, Li ML, Xie X, et al. In vivo imaging and characterization of hypoxia-induced neovascularization and tumor invasion. *Int J Oncol.* 2007;30:45-54.
26. Gerling M, Zhao Y, Nania S, et al. Real-time assessment of tissue hypoxia in vivo with combined photoacoustics and high-frequency ultrasound. *Theranostics.* 2014;4:604-613.
27. Zeng Y, Wang X, Zhang W, et al. Hypertriglyceridemia aggravates ER stress and pathogenesis of acute pancreatitis. *Hepatogastroenterology.* 2012;59:2318-2326.
28. Sah RP, Garg SK, Dixit AK, et al. Endoplasmic reticulum stress is chronically activated in chronic pancreatitis. *J Biol Chem.* 2014;289:27551-27561.
29. Roller C, Maddalo D. The molecular chaperone GRP78/BiP in the development of chemoresistance: mechanism and possible treatment. *Front Pharmacol.* 2013;4:10.

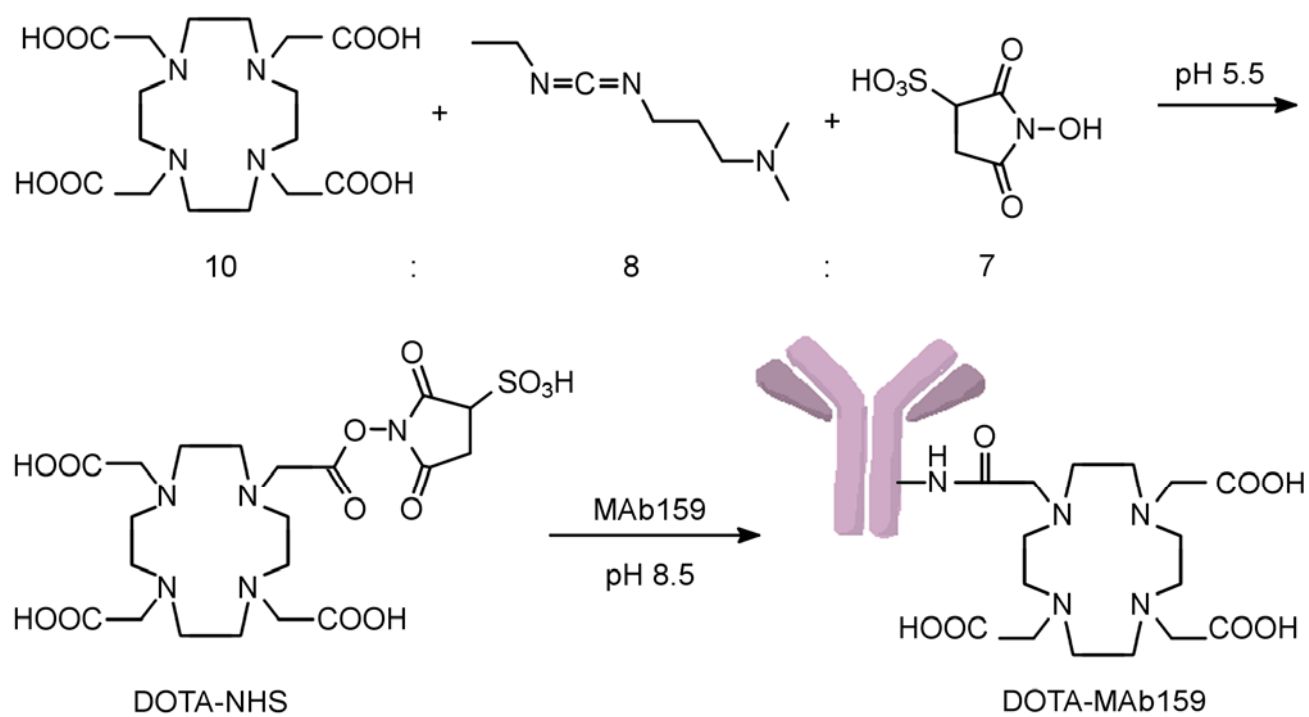


Figure 1. Conjugation reaction for DOTA-NHS and antibody MAb159.

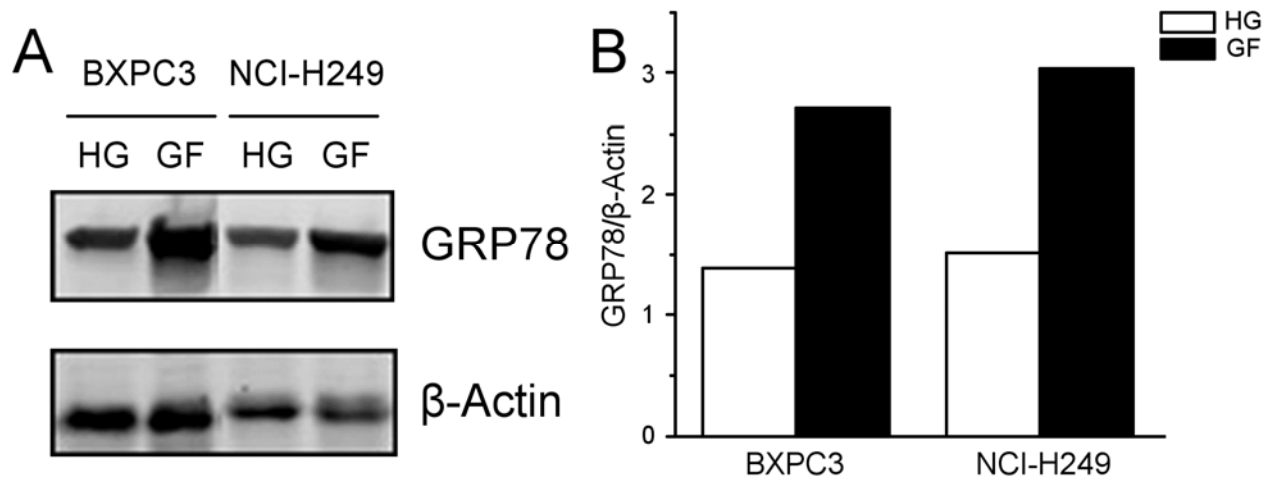
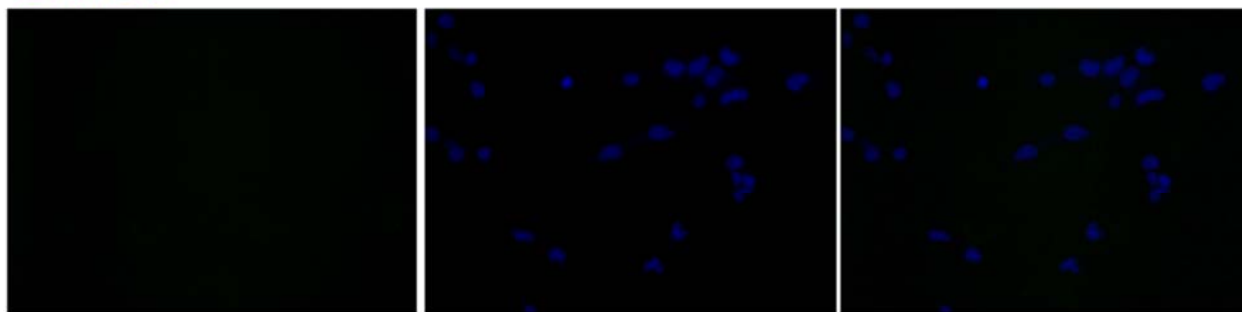


Figure 2. (A) GRP78 protein levels were determined by Western blotting in BXPC3 and NCI-H249 cell lines. The cells were cultured in either high glucose (HG) or glucose-free (GF) DEME supplemented with 10% fetal bovine serum. (B) GRP78/ β -Actin ratio quantification of (A).

BXPC3



BXPC3 + glucose starvation 24 h



Figure 3. Cellular uptake analysis of h159-FAM on BXPC3 tumor cells cultured in either high glucose (HG) or glucose-free (GF) DME supplemented with 10% fetal bovine serum. Scale bar, 100 μ m.

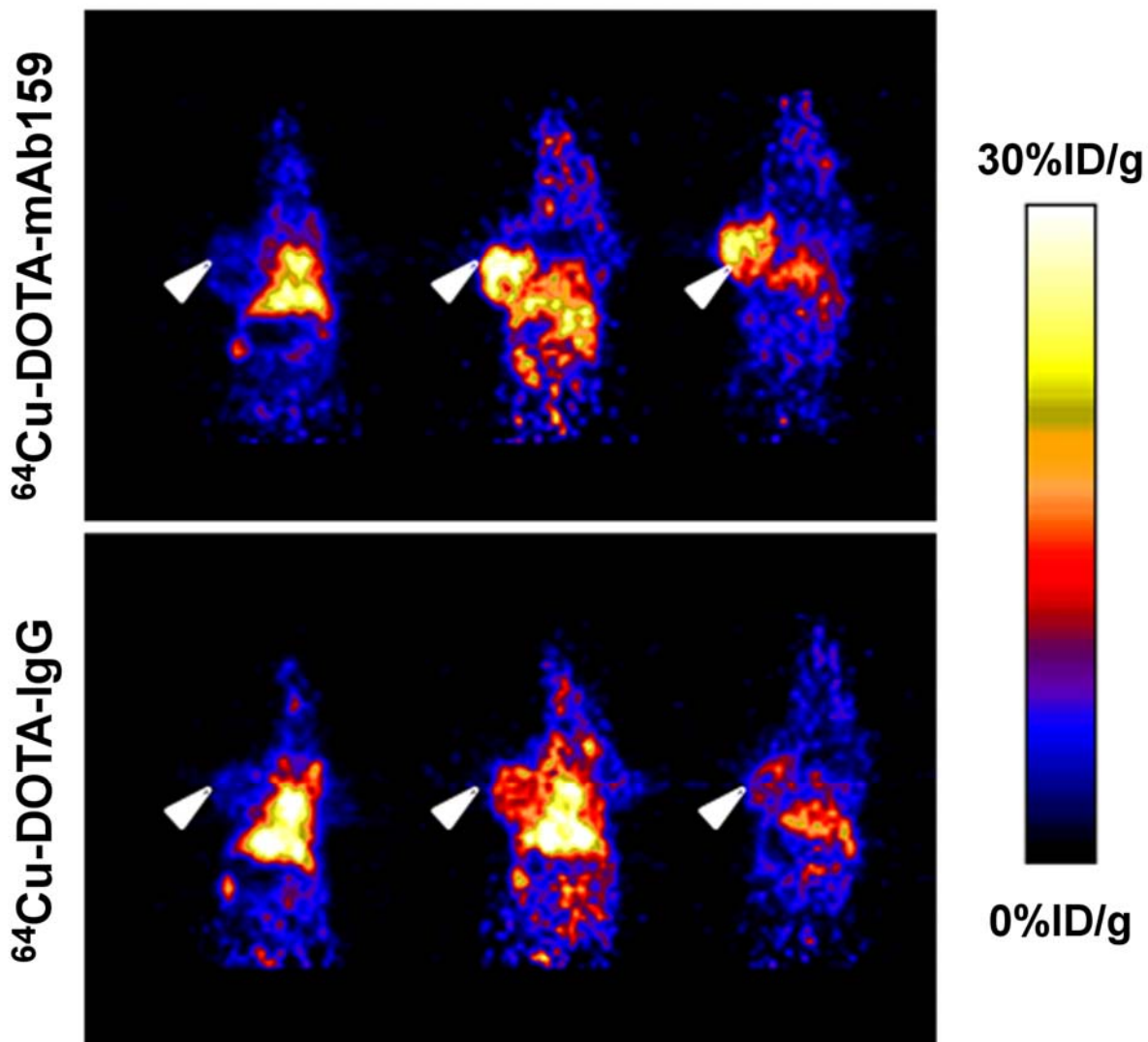


Figure 4. Decay-corrected whole-body coronal small-animal PET static scans of mice bearing BXPC3 tumors. Images were obtained at 1, 17, and 48 h after injection of ^{64}Cu -DOTA-MAb159 (top), ^{64}Cu -DOTA-hIgG (bottom). Arrows indicate tumors.

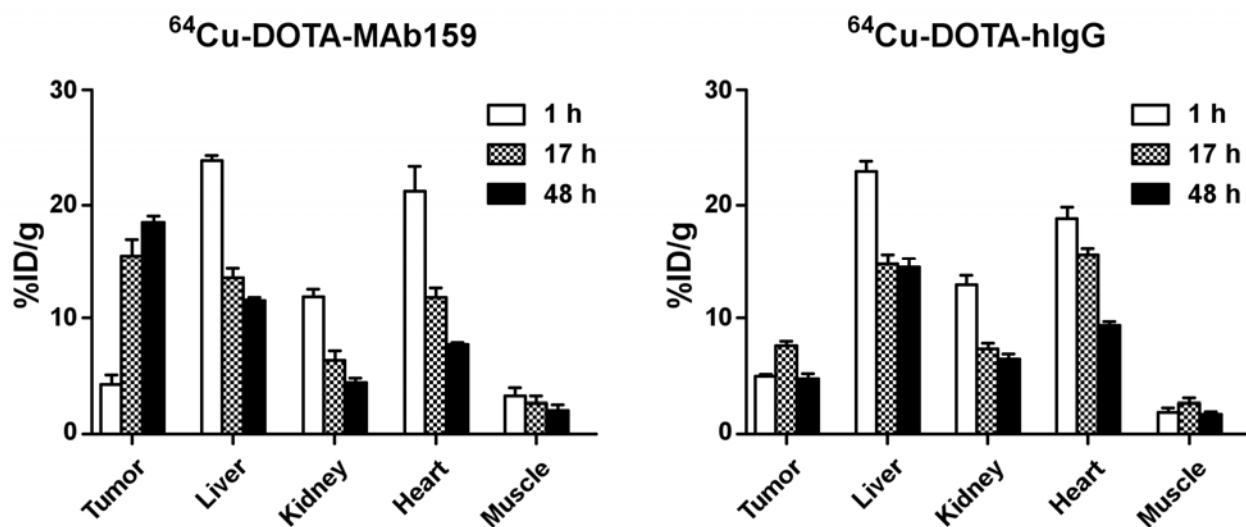


Figure 5. PET quantification of radioactivity in major organs of mice bearing BXPC3 tumors after injection of ^{64}Cu -DOTA-MAb159, ^{64}Cu -DOTA-hIgG.

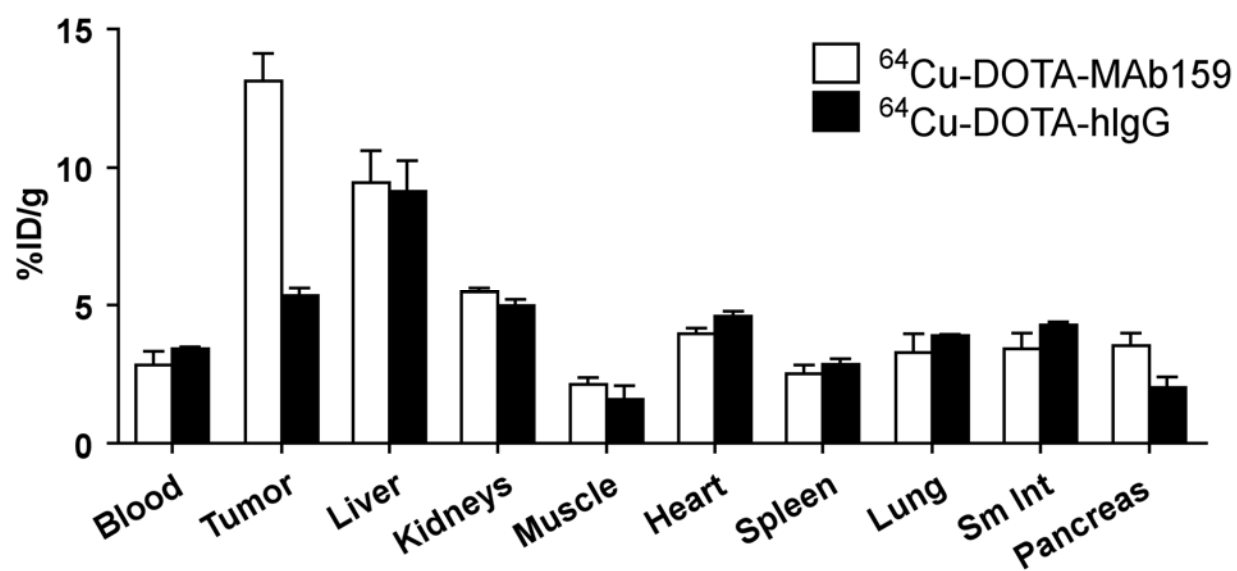


Figure 6. Direct tissue sampling for radioactivity quantification in major organs of mice bearing BXPC3 tumors at 48 h after injection of ^{64}Cu -DOTA-MAb159, and ^{64}Cu -DOTA-hIgG.

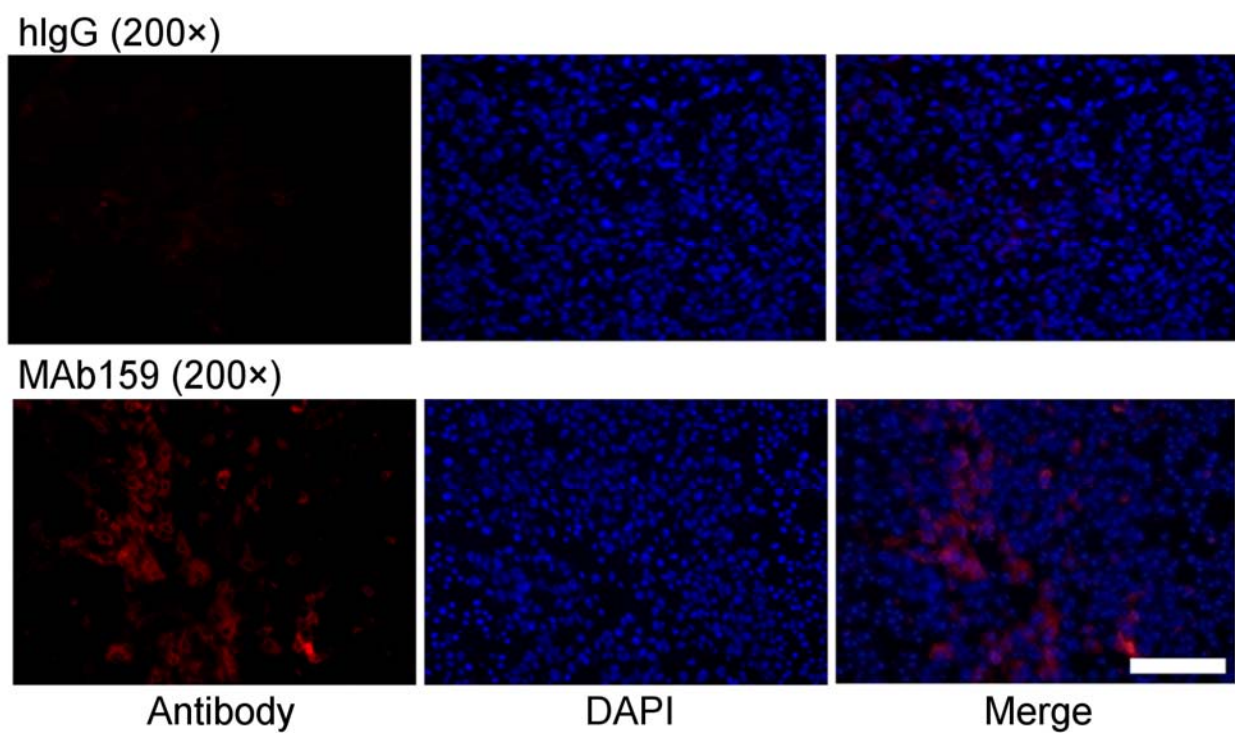


Figure 7. Antibody distribution analysis on BXPC3 tumor sections 48 h p.i. of hIgG or MAb159.

Scale bar, 100 μ m.